Chapter IV

Synthesis of CdS Nanocrystals in Organic phase and Effect of Doping with Manganese and Yttrium

This chapter focuses on the synthesis of cadmium sulphide nanoparticles in chloroform at room temperature. The CdS nanoparticles were rotavapped and then re-dispersed in different organic solvents like toluene, ethanol, etc. The particles were characterized by TEM and XRD (structural characterization) and UV-Vis spectroscopy, Photoluminescence and FTIR measurements (optical characterization). Subsequently, CdS nanoparticles were doped with various levels of manganese and yttrium and effect of doping on the various characteristics was studied.

4.1 Introduction

Development of synthesis protocols for nanomaterials over a range of sizes, shapes and chemical compositions is an important aspect of nanotechnology. In recent years, we have witnessed impressive advances in understanding the unusual physico-chemical and opto-electronic properties of nanomaterials, their synthesis, assembly and packaging for commercial applications [1]. One important area of nanotechnology is involved in the development of reliable processes for the synthesis of nanomaterials over a range of sizes with good monodispersity and chemical composition [2]. Due to high surface area, the nanostructured materials possess a high surface energy and therefore are thermodynamically unstable or metastable. One of challenges in fabrication and processing of nanometerials is to overcome the surface energy and to prevent the aggregation of nanomaterials. Due to high surface energy of the nanoparticles, they are extremely reactive and most systems without protection or passivation of their surfaces undergo aggregation [3]. Organic stabilizers are usually used to prevent nanoparticles from aggregation by capping their surfaces [4].

Metal nanoparticles have attracted considerable interest in fields such as optics and catalysis, because of their size and shape dependent physico-chemical properties [5]. Among such procedures, those that require an aqueous medium are the most convenient to develop because of water's ability to solubilize a variety of ions and stabilizing molecules. On the other hand, nanoparticles prepared in organic media are interesting for applications to catalytic processes and for surface modifications with organic functional groups to fine tune their properties [5-8]. Differently sized and shaped metal nanoparticles can be obtained in organic media either by preparing them directly in those media [9] or by transferring nanoparticles from aqueous phase to organic phases [10-13]. The first approach is very sensitive and difficult to achieve

convenient size and shape controllable processes. The second approach has the advantage that there are many well developed procedures available for the preparation of well-defined metal nanoparticles in aqueous media.

Phase transfer of metal nanoparticles from aqueous phase to an organic phase can be achieved by capping the nanoparticles with thiols and amines [10], or by using phase-transfer reagents, such as surfactants to improve the solubility of nanoparticles in organic media.

CdS is a II-VI semiconductor. CdS nanoparticles exhibit size dependent properties. It has a band gap energy E*g* of 2.42eV [14] at room temperature and pressure. Since CdS has wide band gap, it is used as window material for heterojunction solar cells to avoid the recombination of photo-generated carriers which improves the solar cell efficiency [15]. It has applications in Light Emitting Diodes [16], Photo detectors [17] and sensors [18].

Colloidal particles stabilised with suitable surfactants in volatile organic solvents are particularly attractive since they are known to self assemble into close packed structures on evaporation of the solvent. Growth of colloidal particles involves a two phase approach developed by Brust and Co-workers. They developed a method to produce gold nanoparticles in organic liquids that are not miscible with water. It involves the reaction of a chloro-auric acid solution with tetraoctyl ammonium bromide (TOAB) solution in toluene and sodium borohydride as an anti-coagulant and a reducing agent respectively. TOAB acts as a phase transfer catalyst and a stabilizing agent. To prevent aggregation thiols are used which binds to gold covalently [19]. In a similar work, Kumar et al demonstrate the transfer of cadmium (metal) ions to the organic layer using a phase transfer reagent and thereafter reduced

in the organic medium in the presence of suitable capping agents such as alkane thiols and alkylamines [20].

Mn^{2+} and Y^{3+} ions can be doped in CdS semiconductor host in large proportions without substantially altering the crystallographic quality of the material [21]. Manganese doped CdS nanocrystals have been mainly studied due to the luminescence of the Mn^{2+} ions inside the CdS host. This is due to the fact that Mn^{2+} ions provide good traps for the excited electrons, which give rise to their use in non-linear optics. opto- electronic devices, solar cells, photo detectors and light emitting diodes [22-28]. By doping nanocrystals, the impurity states can play a special role in affecting the electronic energy structure and transient probabilities. In doped nanocrystals, the luminescence quantum efficiency is expected to increase as a result of a greater interaction between the electron and the hole of the host semiconductor with the localised dopant levels [29].

However, effect of Mn doping on the structural phase and size control and optical properties of CdS nanostructures is still an issue and many groups are working on it.

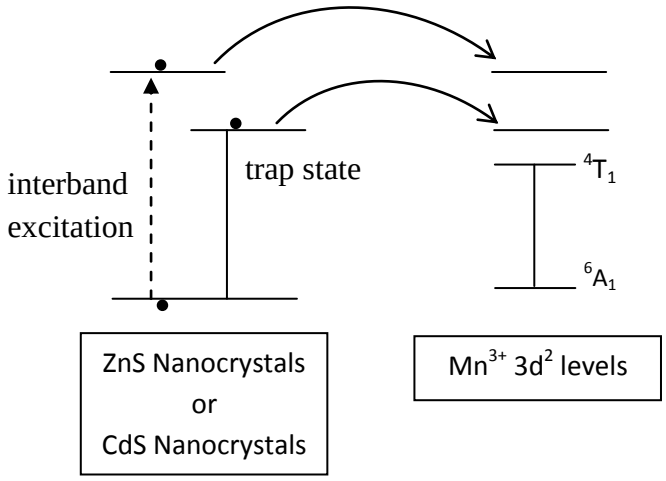

Fig 4.1 *Schematic diagram of the excitation of Mn^{2+} in CdS nanocrystals*

The mechanism of luminescence in CdS: Mn nanostructures can explained as follows: after excitation, energy can be transferred from conduction band of the CdS host to the excited charge carriers which are trapped in shallow trap states. These trapped charge carriers are followed by either energy transfer to the $^4T_1$ excited state of a Mn^{2+} ion (Fig 4.1), or radiative recombination with a deeply trapped hole at a defect state [30].

4.2 Experimental Details

Chemicals:

The following chemicals are used for preparation of the sample. They are of analytical grade and were used as received.

$Cd(NO_3)_2$ - Cadmium Nitrate

$C_{18}H_{36}O_2$ - Stearic Acid

$CHCl_3$ - Chloroform

$C_{18}H_{38}S$ - Octadecane Thiol

$MnCl_2$ - Manganese Chloride

$Y_2(CO_3)_3$ - Yttrium Carbonate

Sample Preparation:

For synthesis, 50 mL of 10^{-3}M aqueous $Cd(NO_3)_2$ solution whose pH was adjusted to 8.5 was mixed with 50 mL of 10^{-3} M stearic acid in chloroform.. The mixture is stirred vigorously using a magnetic stirrer for 5 hours at room temperature.

This leads to the transfer of the cadmium ions from the aqueous phase to the organic phase. The phase transferred cadmium ions present in organic medium were separated from the stirred solution using a separating funnel.

Equal volumes of phase transferred cadmium ions and 5 x 10^{-3} M ODT dissolved in chloroform were added. ODT behaves as a capping agent so that the cadmium ions do not agglomerate.

For standardizing the method of preparation various pH concentrations were experimented. However, for a pH concentration of 8.5, agglomeration was not observed. However, for any pH concentration between 8-9, it was observed that cadmium ions were transferred to the organic phase. The stability of the CdS nanocrystals synthesized was very good for a pH concentration of 8.5. Similarly, the concentration of the capping agent (0.001 M -0.009M) was also varied to optimize the levels of the ODT used for stabilizing the nanocrystals.

The solutions were mixed well by shaking and the mixture was kept aside for 15 minutes. Then H_2S gas was bubbled through the mixture for 15 minutes. As the reaction proceeds, a yellow coloration is observed in the solution, indicating the formation of CdS particles in organic phase.

For Manganese-doping, the corresponding aqueous salts of Mn and Cd were homogenously mixed in required weight proportions.10^{-3}M solution of $MnCl_2$ in proportions of 2%, 4%, 6%, 8%, and 10% in weight proportions are prepared and added along with Cd $(NO_3)_2$ solutions.

Similarly, for doping with yttrium, 10^{-3}M solution of yttrium carbonate dissolved in acidic distilled water and added in proportions of 2%, 4%, 6%, 8% & 10% in weight proportions are prepared and added with $Cd(NO_3)_2$ solution and the same procedure is followed.

Very stable CdS, Cd_{1-x} Mn_xS and CdYS nanocrystals in organic phase with ODT as the capping agents were obtained and the samples were characterised.

4.3 UV- Visible Spectroscopy

Figure 4.2(A), shows the absorption spectra of the CdS nanocrystals in chloroform (organic phase).

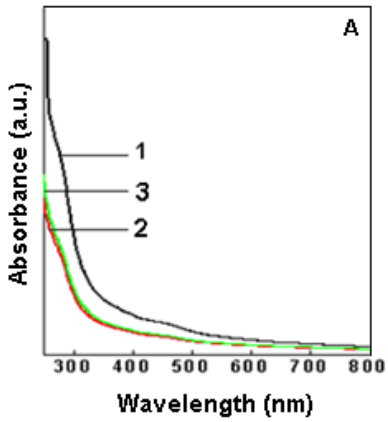

Fig. 4.2 (A) *UV-visible absorption spectra of CdS nanoparticles with different levels of capping agent (ODT) in concentration of 0.005M (1), 0.006M (2) and 0.007 M (3).*

Fig. 4.2(A) shows the UV-visible absorption spectrum of CdS nanoparticles at room temperature with different levels of capping agent (octa decane thiol) in the concentration of 0.005M (curve1), 0.006M (curve2) and 0.007 M (curve3). Subsequently the stability of the nanoparticles was optimized at 0.005 M concentration of ODT.

The preparation produces CdS quantum dots whose structures, composition and electronic structure are well characterized [31]. The absorption is attributed to CdS nanoparticles. The yellow colour of these solutions indicates the formation of CdS nanoparticles. The characteristic excitonic peak centred around 440 nm clearly reveals the quantum confinement effect arising due to small size of as formed CdS nanoparticles The absorption band blue shifts with decreasing size due to quantum size effects.

The absorption edge for 0.005M ODT concentration is found at 250 nm which indicates a blue shift in the absorption edge.

The effective mass approximation formula is given below:

$$E_g\ eff = E_g + \frac{h^2\ \pi^2}{2\ \mu\ R^2} - \frac{1.8\ e^2}{4\ \pi\ \varepsilon_0\ \times R} \qquad \left[\frac{1}{\mu} = \frac{1}{m_{e^*}} + \frac{1}{m_{h^*}}\right]$$

Where,

m_{e^*} - effective mass of electron (0.19 m_e)

m_{h^*} - effective mass of hole (0.8 m_e)

R - radius of particle

ε - dielectric constant

ε_0 - permittivity of free space

The 2nd term is the quantum confinement for electrons and holes which lead to the blue shift [32, 33].

The 3rd term is the Coulomb energy term [34].

The optical band gap can be calculated using the Tauc relation [35]. The well defined peaks are associated with the lowest optical transition, and it provides a simple means to determine the energy gap of the nanocrystals [36].

Fig. 4.2(B) illustrates the absorption spectrum of Cd_{1-x} Mn_xS for different concentrations of manganese.

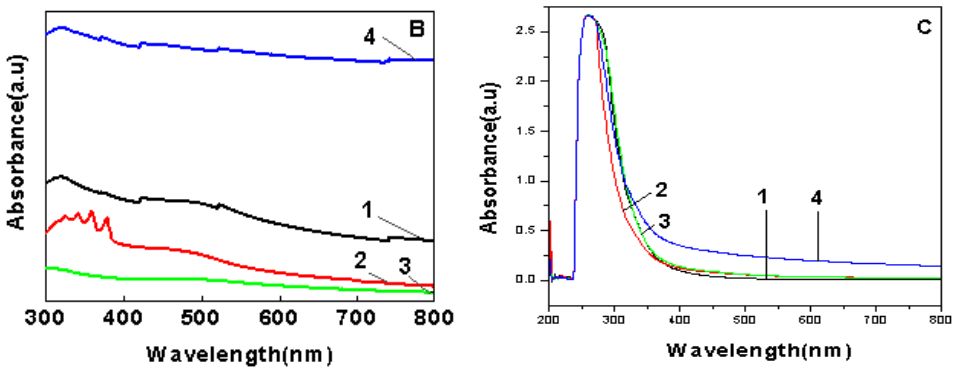

Fig. 4.2 (B) *UV-visible absorption spectra of alloyed $Cd_{(1-x)}$ Mn_xS nanoparticles (1-2% Mn, 2-5% Mn, 3-8% Mn, 4-10% Mn).*

Fig. 4.2(C) *UV – visible absorption spectra of yttrium doped CdS nanoparticles (1-undoped, , 2-2% Y, 3-6% Y, 4-10% Y).*

Figure 4.2(B) shows the absorption spectrum of alloyed $Cd_{0.98}$ $Mn_{0.02}S$ (curve 1), $Cd_{0.95}$ $Mn_{0.05}S$ (curve 2), $Cd_{0.92}$ $Mn_{0.08}S$ (curve 3) and $Cd_{0.90}$ $Mn_{0.1}S$ (curve 4).

The absorption spectrum of CdS: Mn nanocrystals is typical for quantum sized semiconductor nanoparticles with a blue shift of the absorption edge relative to the bulk. The low concentrations of Mn^{2+} ions do not influence the position of the band gap of CdS [37]. The manganese emission in nanocrystals is the result of energy transfer from semiconductor nanocrystal to the manganese ions. On creating the doping of Mn ions, the wavelength was found to shift towards the higher wavelength and the variation in the band gap suggests that there is direct energy transfer between the excited states and the 3d levels of the Mn^{2+} ions that are coupled by energy transfer processes [38].

A strong absorption peak at 320nm is assigned to the optical transition of the first excitonic state of the Cd_{1-x} Mn_xS nanoparticles and its rather narrow shape is an evidence of very small size dispersed particles [39-40].

Figure 4.2(C) shows the absorption spectrum of undoped CdS nanoparticles (curve 1), 2% yttrium doped CdS nanoparticles (curve 2), 6% yttrium doped CdS nanoparticles (curve3) and 10% yttrium doped CdS nanoparticles (curve 4).

The absorption spectrum of yttrium doped CdS nanocrystals is typical of quantum sized semiconductor nanoparticles with a blue shift of the absorption edge relative to the bulk. On doping CdS with yttrium ions, there was a shift towards higher wavelength of the absorption edge and the variation in the band gap suggests

that there is direct energy transfer between the excited states and the 3d levels of the Y^{3+} ions that are coupled by energy transfer processes. A strong absorption peak was found at 270 nm clearly reveals the quantum confinement effect arising due to small size of as formed Yttrium doped CdS nanoparticles, There is no significant shift in the absorption peak of the undoped and the yttrium doped CdS nanoparticles. However, there is a significant change in the values of absorption peaks of the undoped and Mn doped CdS nanoparticles.

4.4 X-Ray Diffraction (XRD)

XRD analysis of the drop coated film on silicon substrates of the organic phase transferred cadmium sulphide nanocrystals, $Cd_{1-x}Mn_xS$ nanoparticles and CdYS nanoparticles was carried out on an Xpert PANalytical instrument operating at 40 kV and a current of 30 mA with CuK_α radiation. These patterns have been recorded within the range of 30˚ - 90˚ with a scan rate of 2˚ / min.

Figure 4.3(A) shows the crystalline XRD pattern of the ODT capped phase transferred CdS nanoparticles obtained in chloroform. The Bragg reflections shown in the diffraction pattern correspond to the face centred cubic structure of zinc blende CdS. The standard values of 2θ are 46.28˚, 51.502˚and 56.066˚ corresponding to lattice planes (110), (103) and (112) respectively (File no. 00-001-0647, Ref code – 00-024-1136) for CdS wurtzite crystal structure. The observed 2θ values are 45.14˚, 51.61˚ and 56.96˚. Thus, the nanocrystalline CdS nanoparticles could be synthesized at room temperature in organic phase showing a peak at 45˚ indicating CdS wurtzite structure.The presence of (110) and (112) planes also supports the existence of hexagonal phase [41].

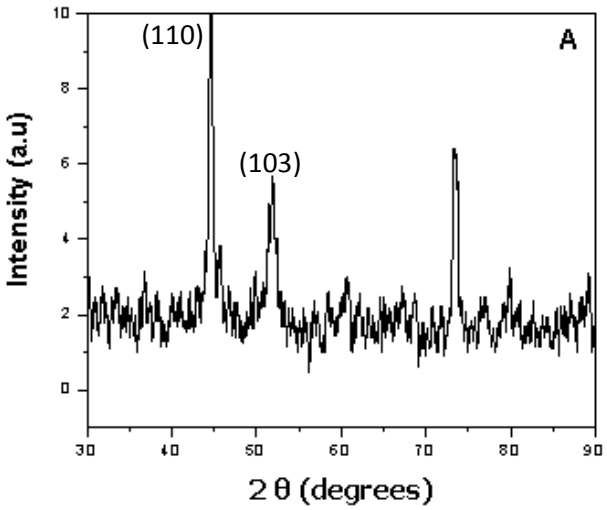

Fig. 4.3(A) ***XRD pattern of drop coated film on Si substrate from synthesized CdS nanoparticles Bragg reflections are indexed.***

Figure 4.3(B) shows the XRD pattern of $Cd_{0.95}Mn_{0.05}S$ nanocrystals synthesized in organic phase. The zincblende phase persists up to 5%-Mn alloying with the CdS nanocrystals. Thus, 5% Mn concentration seems to be perfect for the homogenous formation of alloyed Cd_{1-x} Mn_xS nanocrystals under ambient conditions.

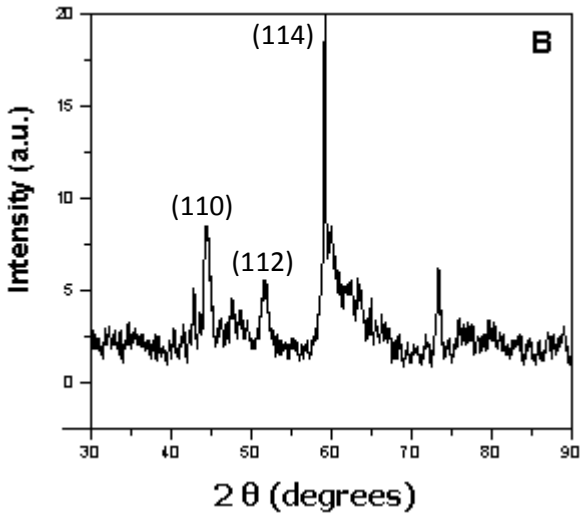

Fig 4.3 (B) ***XRD pattern of drop coated film on Si substrate obtained from $Cd_{0.95}$ $Mn_{0.05}S$ nanocrystals. The Bragg reflections are indexed.***

Figure 4.3(C) shows the XRD pattern of CdYS nanocrystals synthesized in the ratio of Cd/Y being 94/6 %. The most prominent peaks are obtained around 44.56˚

(110) and 59.18˚. Smaller peaks are observed at 52.15˚ (112). The XRD patterns do not show any significant change due to doping with manganese or yttrium into CdS nanocrystals. The crystal structure is in hexagonal phase [41].

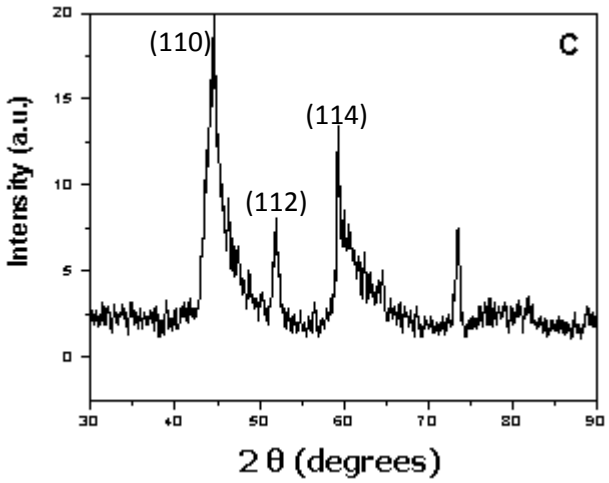

Fig. 4.3(C) ***XRD pattern of drop coated film on Si substrate obtain from $Cd_{0.94}$ $Y_{0.06}S$ nanocrystals. The Bragg reflections are indexed.***

4.5 Fluorescence Spectroscopy

Room temperature fluorescence spectra (excitation at 350 nm) for the samples of CdS, 5% manganese doped Cd_{1-x} Mn_xS with chloroform, ethanol and toluene solvents are studied and shown in fig 4.4(A), 4.4(B), 4.4(C) and 4.4(D).

All chemical compounds absorb energy which causes excitation of electrons bound in the molecule, such as increased vibrational energy or, under appropriate conditions, transitions between discrete electronic energy states. For a transition to occur, the absorbed energy must be equivalent to the difference between the initial electronic state and a high-energy state. This value is constant and is characteristic of the molecular structure. This is termed the excitation wavelength. If conditions permit, an excited molecule will return to ground state by emission of energy through heat and/or emission of energy quanta such as photons.

Fluorescence occurs when a molecule absorbs photons from the UV-visible light spectrum (200-900 nm), causing transition to a high-energy electronic state and then emits photons as it returns to its initial state. Some energy, within the molecule, is lost through heat or vibration so that emitted energy is less than the exciting energy; i.e., the emission wavelength is always longer than the excitation wavelength. The difference between the excitation and emission wavelengths is called the Stokes shift.

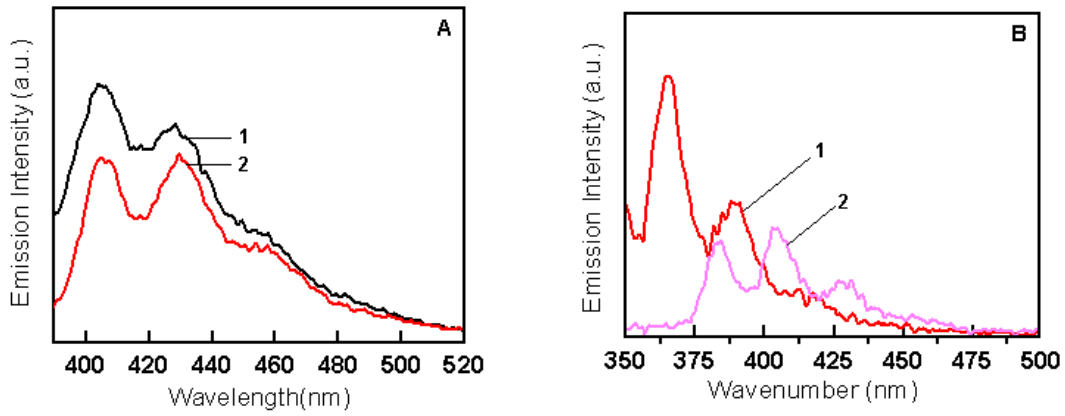

Fig. 4.4(A) ***Fluorescence emission spectra recorded from ODT capped CdS nanoparticles in chloroform with excitation wavelength of 350nm (1) and 380nm (2).***

Fig. 4.4(B) ***Fluorescence emission spectra of ODT capped $Cd_{0.95}$ $Mn_{0.05}S$ nanoparticles in chloroform with excitation wavelengths 350nm and 380nm (1) and 320nm (2).***

In figure 4.4(A) the excitation wavelength for curve 1 is 350 nm and for curve 2 the excitation wavelength is 380 nm. Fluorescence emission spectra of CdS nanoparticles are studied with chloroform as solvent.

Figure 4.4(B) illustrates the fluorescence spectra of $Cd_{0.95}Mn_{0.05}S$ nanoparticles with chloroform as the organic solvent. Curve 1 refers to the spectra for excitation wavelength 350 nm and 380 nm. Curve 2 refers to the fluorescence spectra for excitation wavelength of 320 nm.

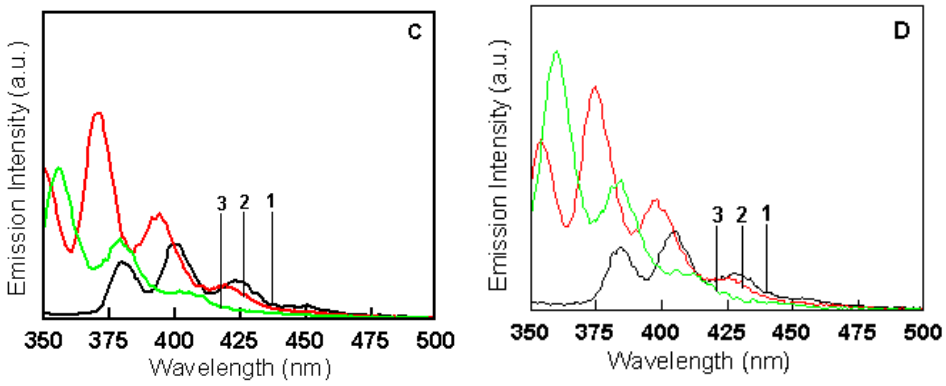

Fig. 4.4(C) ***Emission spectra of ODT capped $Cd_{0.95}$ $Mn_{0.05}S$ nanoparticles in ethanol with excitation wavelengths 320 nm (1), 350 nm (2), 365 nm (3).***

Fig. 4.4(D) ***Emission spectra of ODT capped $Cd_{0.95}$ $Mn_{0.05}S$ nanoparticles in toluene with excitation wave lengths 320 nm (1), 350 nm (2), 36 5nm (3).***

Figure 4.4(C) illustrates the fluorescence spectra of $Cd_{0.95}$ $Mn_{0.05}S$ nanoparticles in ethanol solvent. Curve 1 refers to the spectra for excitation wavelength 320 nm; curve 2 illustrates the fluorescent spectra with excitation wavelength of 350nm. Curve 3 refers to the fluorescence spectra for excitation wavelength of 365 nm.

Figure 4.4(D) illustrates the fluorescence spectra of $Cd_{0.95}$ $Mn_{0.05}S$ nanoparticles in toluene solvent. Curve 1 refers to the spectra for excitation wavelength 320 nm; curve 2 illustrates the fluorescent spectra with excitation wavelength of 350 nm. Curve 3 refers to the fluorescence spectra for excitation wavelength of 365 nm.

The characteristic emission observed for the phase transferred CdS nanoparticles lies in the visible region of 400 nm – 520 nm. The peak is centred at 405 nm corresponds to the bandgap or near band gap emission resulting from recombination of electron hole pairs. The broader emission band at 427 nm is assigned to the charge carrier recombination from electrons trapped at the surface defects. The deep trap emission occurring at 430 nm allows the trapping of electrons

and holes at the surface trap sites nonradiatively and gives low energy trap emission usually with low quantum yield.

Similarly, the fluorescence measurements on $Cd_{(1-x)}$ Mn_xS nanocrystals in organic phase suggests clear enhancement in the band edge emission characteristic compared to the undoped CdS nanoparticles as shown in fig. 4.4(B). The characteristic emission observed for phase transferred 5% Mn doped CdS nanoparticles lie in the visible range of 350 nm to 500 nm.

$Cd_{0.95}$ $Mn_{0.05}S$ with chloroform as solvent exhibits a broad feature at 365 nm. A significant shift in the peak position is observed in the spectra of $Cd_{(1-x)}$ Mn_xS. The cause for this blue shift in the emission spectra is thought to be an indication that the quantum confinement length is primarily defined by particle width and its difference between the widths of the various particles. The surface state saturation is modified by particle-surfactant interaction. It can be inferred that the quenching of the fluorescence can be altered by changing the cadmium concentration. The CdMnS nanoparticles synthesized in chloroform was rotavapped and then redispersed in ethanol and toluene..

There is no significant shift in the value of the peak intensity and secondary feature when the $Cd_{(1-x)}Mn_xS$ nanocrystals are dispersed in chloroform, ethanol and toluene. Fig. 4.4(A), (B), (C) and (D) also illustrate the peak emission intensities for other excitation wavelengths like 320 nm and 365 nm. The maximum emission intensity is obtained for 350 nm excitation.

4.5 Fourier Transform Infra Red Spectroscopy

FTIR measurements have been made in the wave number range 1000 cm^{-1} and 4000 cm^{1}. Fig. 4.5(A) illustrates the FTIR measurements of undoped CdS (curve 1), 5% manganese doped cadmium sulphide (curve2). Fig. 4.5(B) illustrates the FTIR measurements of undoped CdS (curve 1) and yttrium doped Cadmium sulphide with doping levels of 2% (curve 2), 6% (curve 3) and 10% (curve 4).

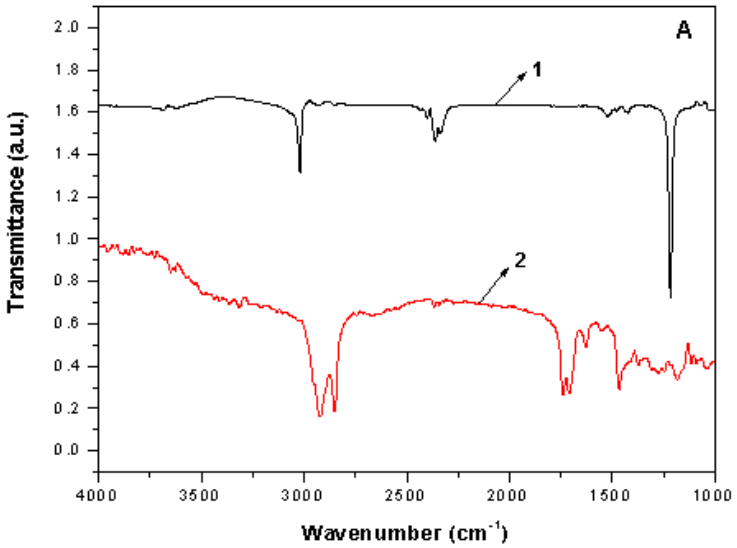

Fig. 4.5(A) ***FTIR spectra recorded from drop coated film on Si(111) wafer of CdS nanoparticles (1) and 5% Mn doped CdS nanocrystals (2).***

CdS particles showed characteristic absorptions in the symmetric stretching band in the range of 2900-3000 cm^{-1} associated with C-H stretching. Strong band positions 1200-1300 cm^{-1} are possibly due to stretching vibrations of the sulphate group.

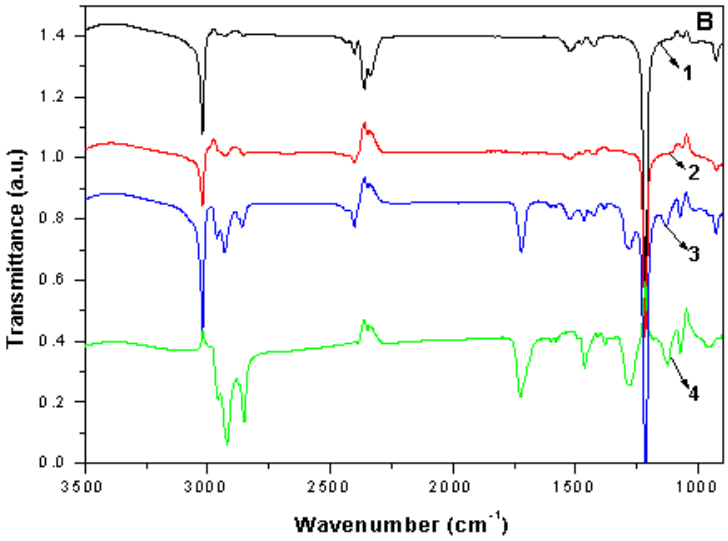

Fig. 4.5(B) ***FTIR spectra recorded from drop coated film on Si(111) wafer of CdS nanoparticles (1), 2% Y doped CdS nanocrystals (2), 6% Y doped CdS nanocrystals (3) and 10% Y doped CdS nanocrystals (4).***

CdS particles showed two stretching bands asymmetric and symmetric between 2900-3000 cm^{-1} are associated with C-H stretching. Weak vibrations in the range of 2250-2300 cm^{-1} are due to the strong binding of the yttrium with Cd-S bond Very weak bending vibrations appeared at 1600 cm^{-1} due to C-C stretching .Weak absorption bands near 1750 cm^{-1} are assigned to the C-O carboxylic stretch. Strong band positions 1200-1300 cm^{-1} are possibly due to stretching vibrations of the sulphate group. There are strong to medium absorption bands between 600-700 cm^{-1} are assigned to Cd-S stretching.

4.6 Particle Size Distribution

Dynamic Light Scattering (DLS), is the only technique able to measure particles in a solution or dispersion in a fast, routine manner with little or no sample preparation. DLS is based on Photon Correlation Spectroscopy and has the advantages of small measurement times, typically in seconds or at most a few minutes, with the sample having been through the minimum of preparation. The minimal or entire lack

of sample preparation ensures that the sample is measured as it actually is. The preparation required for other techniques can change the properties of the particles, for example aggregates can be created or destroyed.

The Particle Size Distribution (PSD) of Cadmium Sulphide nanoparticles in organic phase is in the range of 100 nm - 200 nm size. About 80% of the particles have a size less than 150 nm. Figure 4.6 (A) shows the particle size distribution of undoped CdS nanoparticles.

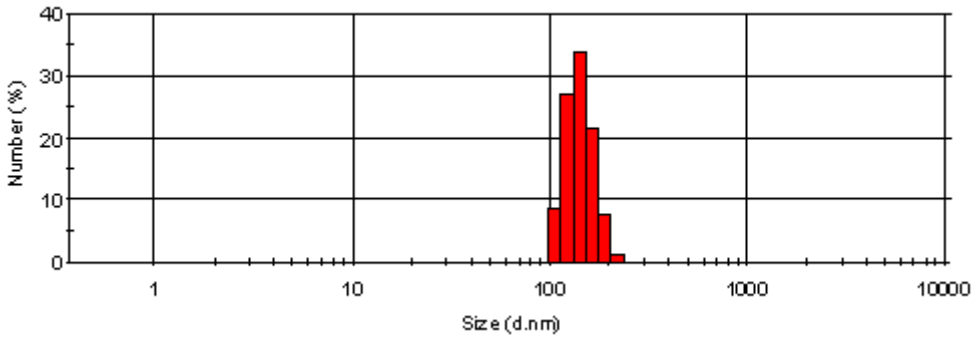

Fig. 4.6(A) ***Histograms showing particle size distribution of ODT capped CdS nanoparticles.***

Similarly, the particle size distribution of Cadmium sulphide doped with manganese for $Cd_{0.95}$ $Mn_{0.05}S$ was also measured. The fig. 4.6(B) illustrates the distribution. The nanoparticles synthesized are in the range of 200-300 nm size.

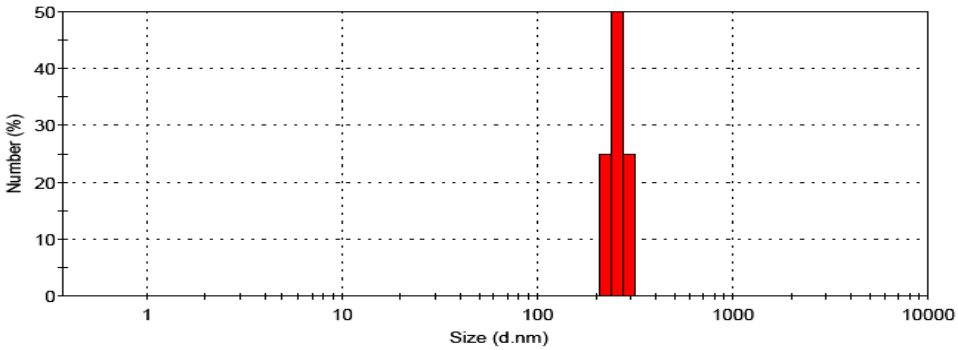

Fig. 4.6(B) ***Histograms showing particle size distribution of ODT capped $Cd_{0.95}$ $Mn_{0.05}S$ nanoparticles.***

Figure 4.6(C) shows the PSD of the phase transferred cadmium sulphide with 6% of yttrium. This seems to be the optimum level of doping since the size of the nanoparticles is in the range of 70-120 nm. 90% of the particles are in the size range of 90 nm – 120 nm. As the doping level further increases the size of the particles also increases.

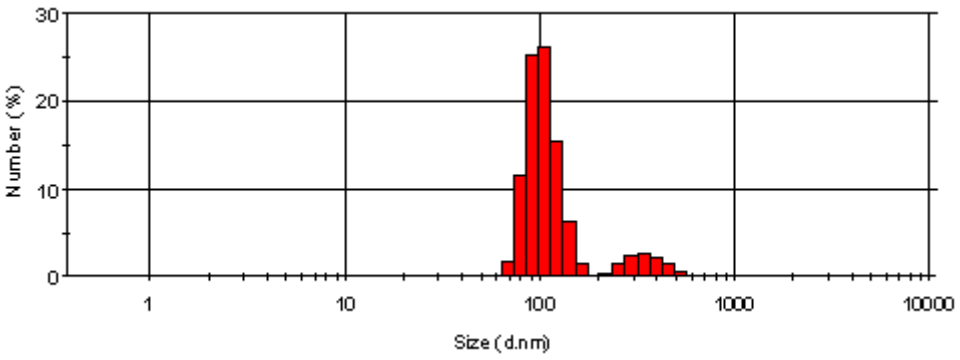

Fig 4.6 (C) ***Histograms showing particle size distribution of ODT capped*** $Cd_{0.94}$ $Mn_{0.06}S$ ***nanoparticles.***

4.7 Transmission Electron Microscopy (TEM) Measurements

Figure 4.7 shows the TEM micrographs recorded at different magnifications from as prepared phase transferred CdS nanoparticles in chloroform.

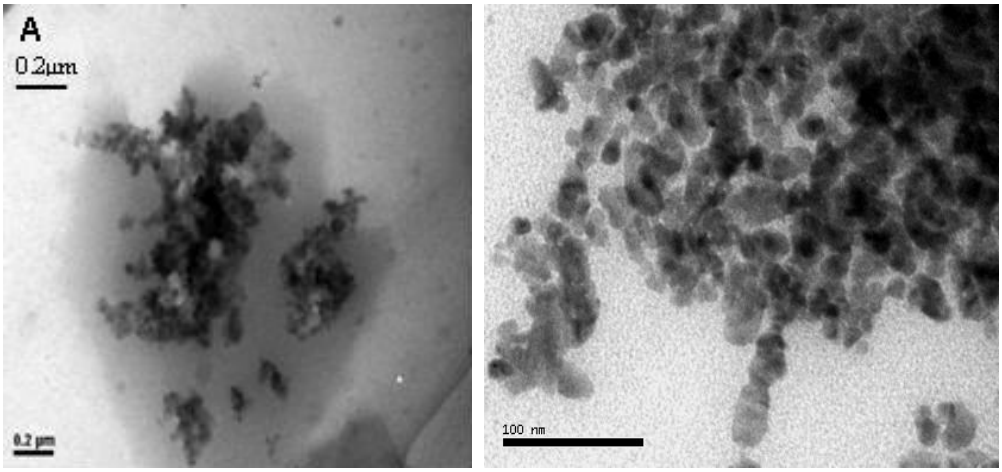

Fig. 4.7 ***TEM micrographs recorded at different magnifications from a drop coated film of ODT capped CdS nanoparticles.***

Ribbon like CdS nanostructures capped with ODT is clearly seen in Fig. 4.7(B). This strongly suggests the strong surface binding of the ODT molecules with CdS nanoparticles thus restricting their aggregation. Fig. 4.7(A) shows spherical nanoparticles under assembly into superstructures of variable morphology that were found to be uniformly distributed. The CdS nanoparticles were observed to form monolayers of honey comb like structure. Thus the morphology of the CdS nanoparticles synthesized varies from spherical to flat, ribbon like structures and plate like structures. They indicate the polycrystalline nature of the semiconductor nanoparticles.

Figure 4.8 shows the High Resolution TEM (HRTEM) micrographs recorded at different magnifications from as prepared phase transferred CdYS nanoparticles with a doping concentration of 6% in chloroform.

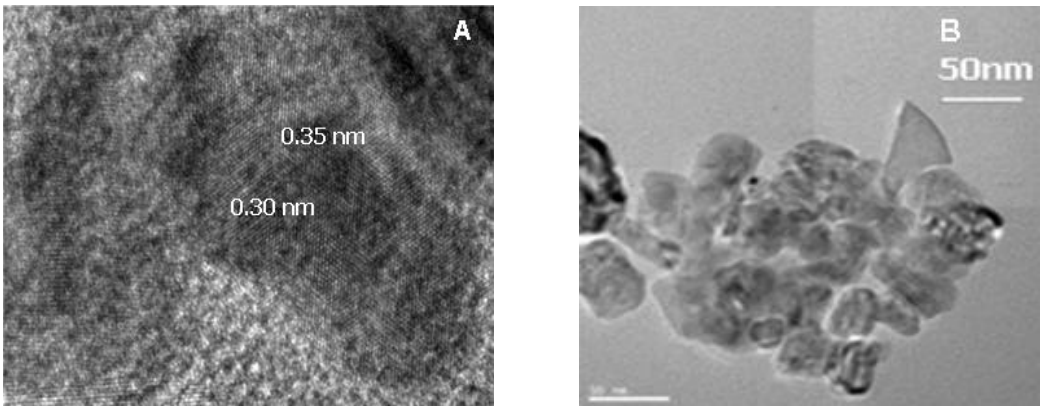

Fig. 4.8 ***TEM micrographs recorded at different magnifications from a drop cast film of ODT capped $Cd_{0.94}$ $Y_{0.06}$S nanoparticles.***

The micrographs suggest that spherical nanoparticles having superstructures of variable morphology are found to be distributed in the solution. The average size of the quantum dots depends on the amount of capping agents used in the preparation.

Pyramid like structure showing the polycrystalline structure were synthesized. Generally, a higher amount of capping agent produces smaller QDs. It can be observed that the size of the nanoparticles is in the range of 20-40 nm.

4.8 Photoluminescence (PL) measurements

For a typical nanoparticle sample, luminescence can be generally divided into band gap emission, which includes excitonic emission and trap state emission.

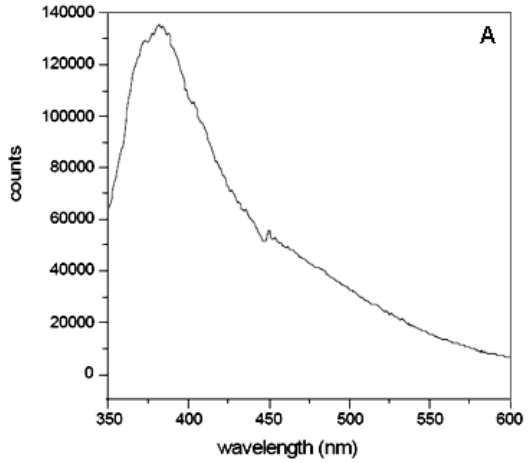

Fig. 4.9(A) ***PL spectra of ODT capped CdS nanocrystals recorded with excitation wavelength of 325 nm*****.**

Photoluminescence measurements of undoped CdS nanocrystals in organic phase at an excitation wavelength of 325 nm is shown in Fig. 4.9 (A) and 5% Mn doped CdS nanoparticles were done at different excitation wavelengths at 270 nm, 330 nm and 360 nm. The emission peak at 3eV is dominant in all spectra. The PL spectrum shown consists of broad emission peaks at 375 nm for CdS. The PL spectra shows three peaks namely band edge, shallow and deep traps. For 5% manganese doped CdS, there is an increase in PL intensity and also a shift in the wavelength in all the bands such as 390 nm, 410 nm and 440 nm when excited with laser of 270 nm as shown in Fig. 4.9 (B).

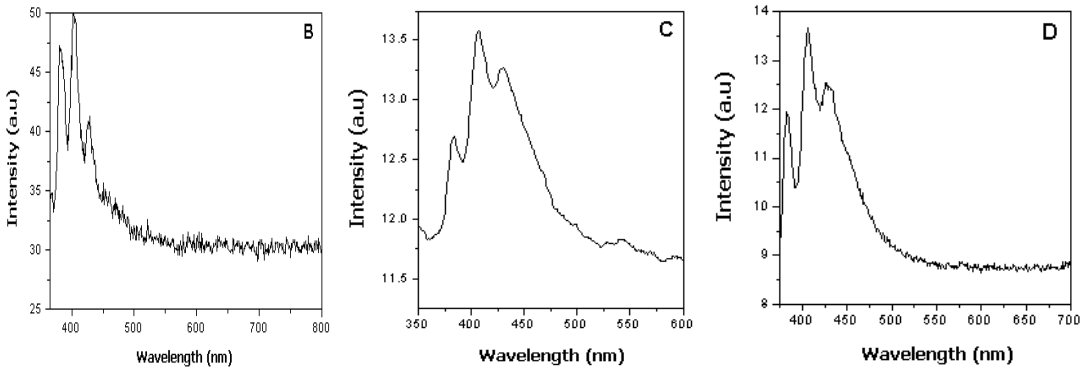

Fig. 4.9 ***PL spectra of ODT capped $Cd_{0.95}$ $Mn_{0.05}S$ nanocrystals recorded with excitation wavelength of 270 nm (B), 330 nm (C) and 360 nm (D).***

When the excitation wavelength is 330 nm / 360 nm as shown in Fig. 4.9(C) and Fig. 4.9 (D), the wavelength of emission remains the same.

The trap states are located within the semiconductor band gap and the emission is usually red shifted relative to the band edge emission. In addition the trap state luminescence is often characterized by a large bandwidth reflecting a broad energy distribution of the emitting states. The characteristic luminescence can consist of relatively sharp emission bands having spectral widths of few nms, but also of broad bands, whose width can exceed 50 nm in visible part of the spectrum. Sharp emission bands are characteristic of optical transitions between electronic states in chemical bonding. These activities in the host material define the luminescence efficiency and can produce a narrowing or a broadening of the bandwidth of the spectra [41].

The PL band mostly related to the intrinsic emission of Mn^{2+} ions significantly shifts with respect to the absorption edge. This variation in the peak energy may be attributed to surface defects [42]. The observable red emission caused by manganese ions located within the CdS is frequently noticed for nanocrystalline semiconductors. The emission from the first excited state to the ground state decides the position of the band strongly depending on the host lattice.

The PL spectra of undoped CdS and yttrium doped CdS in organic phase is shown in fig. 4.10 (A) and 4.10 (B) with different excitation wavelengths 325 nm and 380 nm.

In fig 4.10 (A) the excitation energy 3.8eV (325 nm) is larger than the energy gap of the material (approx 2.8eV) [43], so a strong luminescence from the electron hole recombination is expected. Similarly for the excitation energy of 3.2eV (380 nm), a strong luminescence due to electron hole recombination is expected. Also due to the presence of various energy levels inside the band gap region, a strong luminescence is expected. The defect mode at about 2.7 eV is dominant in almost all spectra. Curve 1 refers to undoped CdS, curve 2 refers to CdS doped with 2% concentration of yttrium, Curve 3 refers to CdS doped with 6% concentration of yttrium and curve 4 refers to CdS doped with 10% concentration of yttrium.

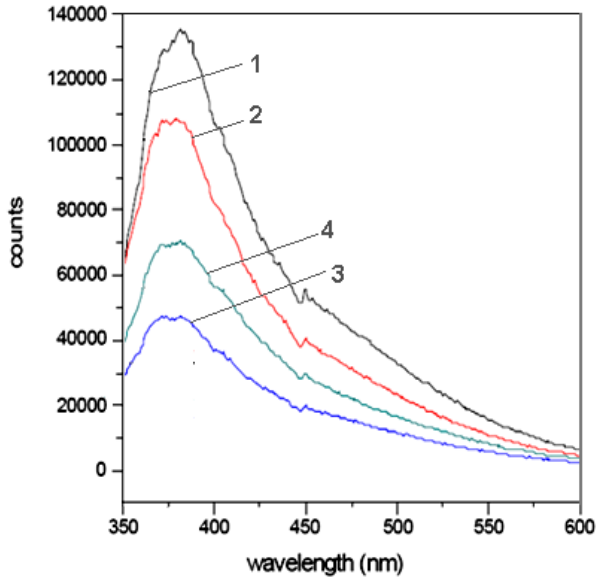

Fig. 4.10(A) ***PL spectra of ODT capped CdS nanoparticles (1), $Cd_{0.98}Y_{0.02}S$ nanoparticles (2), $Cd_{0.94}Y_{0.06}S$ nanoparticles (3), $Cd_{0.9}Y_{0.1}S$ nanoparticles(4) at an excitation wavelength of 325 nm.***

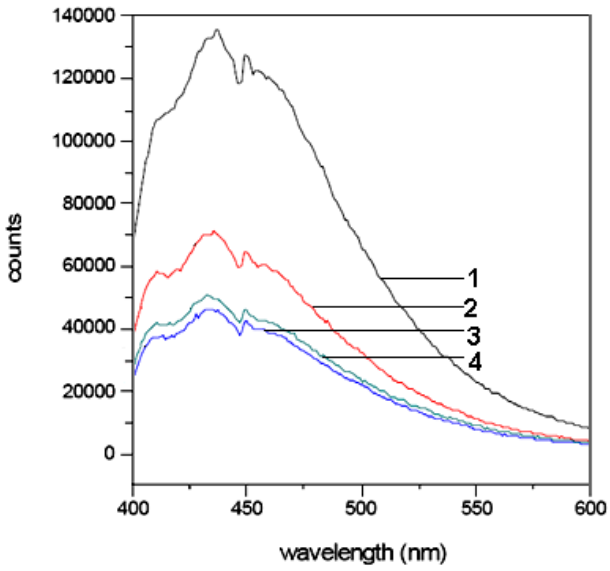

Fig. 4.10 (B) ***PL spectra of ODT capped CdS nanoparticles (1), $Cd_{0.98}$ $Y_{0.02}S$ nanoparticles (2), $Cd_{0.94}Y_{0.06}S$ nanoparticles (3), $Cd_{0.9}Y_{0.1}S$ nanoparticles(4) at an excitation wavelength of 380 nm.***

It can be found that the luminescence spectra for all the samples are contributed due to two individual components, which correspond to band edge emission and surface trap emission. After excitation, energy will be transferred from the conduction band of the CdS host to the excited charge carriers which are trapped in shallow trap states. These trapped charge carriers are followed by energy transfer of excited state of Y^{3+} ion or radiative recombination with a deeply trapped hole at a defect state. The trap states are located within the semiconductor band gap and hence their emission is red shifted relative to the band edge emission.

4.9 Zeta potential measurements

Zeta potential is one of the main forces that mediate inter-particle interaction. Most particles acquire a surface charge, principally either by ionization of surface group or adsorption of charged species. These surface charges modify the distribution of the surrounding ions, resulting in a layer around the particle that is different to the bulk solution.

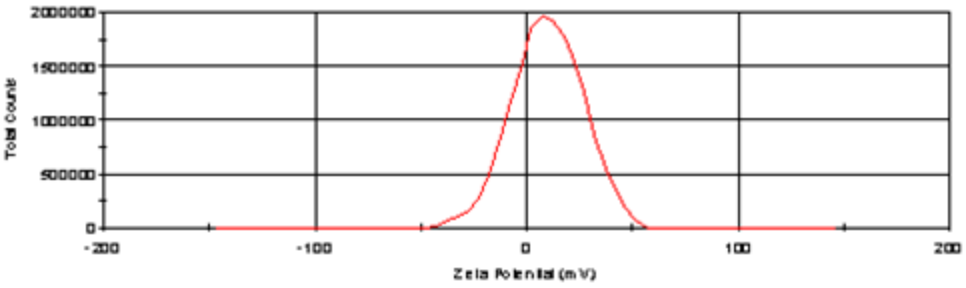

Fig. 4.11 ***Plot showing the zeta potential of ODT capped CdS nanoparticles in chloroform***

The zeta potential is the potential at the point in this layer where it moves past the bulk solution. It is the potential difference between the dispersion medium and the stationary layer of the fluid attached to the dispersed particle. When any object, solid particle, liquid droplet or a gas bubble, is placed into a liquid, a double layer appears on the object. The double layer refers to two parallel layers of charge surrounding the object. The first layer (surface layer) consists of ions adsorbed due to chemical interaction with the object. The second layer (diffuse layer) made of free ions which move in the fluid due to the influence of electrical attraction and thermal motion.The charge at this plane/layer is sensitive to the concentration and type of ions in solution. For molecules and particles that are small enough and of low enough density to remain in suspension, a high zeta potential will confer stability i.e. the solution or dispersion will resist aggregation.

The zeta potentials measured for undoped CdS shows a slight positive potential of 10-15 *m*V indicating instability (Fig. 4.11). The distribution shown does not show any significant zeta potential. This is possibly due to the use of chloroform as a solvent which is non polar in nature.

4.10 Summary

- It has been shown that Cadmium ions present in aqueous medium can be transferred into non polar organic solvent and CdS sulphide nanocrystals in coordination with ODT molecules present in organic

phase can be obtained. This approach is promising for growing heterocolloidal particle assemblies of quantum dots.

- UV-vis absorption and the band edge photoluminescence spectra are consistent with narrow size distribution and excellent particle quality.
- The XRD pattern of the ODT capped phase transferred CdS nanoparticles obtained in chloroform show that the diffraction pattern correspond to the face centred cubic structure of zinc blende CdS.
- The produced quantum dots are fairly uniform and are spherical in nature. The micrographs suggest that the nanoparticles exhibit polycrystalline structure.
- The study of Malvern's particle size analysis reflects the average size of the nanoparticles synthesized. Doping with yttrium effects quantum confinement of the particles.

The synthesis of CdS nanocrystals in organic phase and the enhancement of the luminescence due to doping with manganese and yttrium can contend to be the core materials for the development of Organic LEDs.

4.11 References

[1] *"Scientific American"* discusses exciting developments in the field of nanotechnology and current / futuristic applications envisaged for nanomaterials, **Sept**. **2001.**

[2] Sastry, M. "Phase transfer protocols in nanoparticles synthesis" – *Current Science*, **Dec. 2003**.

[3] Vllman, A. *Chem Rev.,* **1996,** *96, 1533***.**

[4] Tang, H.; Mi Yan; Hui Zhang; Xin, M.; Yang, D. *Materials Letter,* **2005,** *59, 1024.*

[5] El-Sayed, M.A. *Acc. Chem. Res*., **2001**, *34, 257.*

[6] Kumar, A.; Mandal, S.; Mathew, S.P.; Selva Kannan, P.R.; Mandake, A.B.; Chaudhari, R.; Sastry, M. *Langmuir*, **2002**, *18, 6478.*

[7] Shipway, A.N.; Willner, I. *Chem Commun*., **2001**, *2035.*

[8] Yamada, M.; Kuzume, A.; Kurihara, M.; Kubo, K.; Nishihara, H. *Chem Commun.*, **2001**, *2476.*

[9] Left, D.V.; Brandt, L.; Heath, J.R. *Langmuir*, **1996**, *12, 4723.*

[10] Wang, W.; Efrima, S.; Regev, O. *Langmuir*, **1998**, *14, 602*.

[11] Lala, N.; Lalbegi, S.P.; Adyanthaya, S.D.; Sastry, M. *Langmuir*, **2001**, *17, 3766*.

[12] Liu, J.; Alvarez, J.; Ong, W.; Roman, E.; Kaifer, A.E. *J. Am. Chem. Soc.*, **2001**, *123, 11148.*

[13] Yao, H.; Momozawa, O.; Hamatani, T.; Kimura, K., *Chem. Mater.*, **2001**, *13, 4692*.

[14] Krishnan Rajeshwar; Norma R. de Tacconi; Chenthamarakshan, C. R. *Chem. Mater*, **2001,** *13, 2765*.

[15] Arturo Morales – Acevedo, *Solar Energy Materials and Solar Cells*, **2006,** *90, 2213*.

[16] Murai, H.; Abe, T.; Matsuda, J.; Sato, H.; Chiba, S.; Kashiwaba, Y. *Appl. Surf. Sci*, **2005,** *244, 351*.

[17] Wang, Y.; Ramanathan, S.; Fan, Q.; Yun, F.; Morkoe, H.; Bandyopadhyay, S. *J. Nanoscience Nanotechnology,* **2006,** *6(7), 2077*.

[18] Ponzoni, A.; Comini, E.; Sberveglieri, G.; Zhou, J.; Deng, S. Z.; Xu, N. S.; Ding, Y.; Wang, Z. L. *Appl Phys Lett.,* **2006,** *88, 203101*.

[19] Brust, M.; Walker, D.; Bethell, D.; Schiffrin, D.J.; Whyman, R., *J. Chem. Soc., Chem Commun.*, **1994**, *801*.

[20] Ashavani Kumar, Mandale, A. B.; Sastry, M. *Langmuir***, 2000**, *16, 9299.*

[21] Furdyna, J.K.; Kossut, *J. Semiconductors and Semimetals*, 25, Academic Press, New York, **1988**.

[22] Tripathi, B.; Singh, F.; Avasthi, D.K.; Das, D.; Vijay, Y.K. *Physica B* **2007**, *400, 70*.

[23] Lotfi Orimi, R.; Shahtahmasebi, N.; Tajabor, N., *Physica E* **2008**, *40, 2894*.

[24] Tanaka, M.; Masumoto, Y., *Solid State Commun.* **2001**, *120, 7*.

[25] Peyghambarian, N.; Koch, S.W.; Mysyrowicz, A. *Introduction to semiconductor optics*, Prentice Hall, Engle wood cliffs, NJ, **1993**.

[26] Herz, E. *M.Sc. Thesis*, Virginia Polytechnic, Virginia, **2003**.

[27] Sh. Liu; Liu, F.; Guo, H., *Solid state commun.*, **2000**, *115, 615*.

[28] Nanda, J.; Kuruvilla, B.A.; Sarma, D.D., *Phys. Rev. B* **1999** , 59 *7473*.

[29] Brus, L.E. *J. Chem. Phys*. **1983**, *79, 5566*.

[30] Tanaka, M. *J. Lumin.,* **2002**, *100 ,163*

[31] Petit, C.; Lixon, P.; Pileni, M. P. *J. Phys. Chem*, **1990**, 94, 1598.

[32] Efroz AIL; Efroz, A. L.; *Fiz Tekh Poluprovodn* ,**1982,** *16, 1209*.

[33] Efroz AIL; Efroz, A. L. *Sov. Phys. Semiconductor*, **1982**, *16, 772*.

[34] Brus, L. E. *J. Chem. Phys.,* **1984,** *80, 4403*.

[35] Tauc, J. (Ed) *Amorphous and Liquid semiconductors*, Plenum Press, New York, **1974**.

[36] Spanhel, L.; Hasse, M.; Weller, H.; Henglein, A. *J. Am. Chem. Soc.,* **1987,** *109 , 5649.*

[37] Ikeda, M.; Itoh, K.; Sato, H. *J. Phys. Soc. Jpn.*, **1968,** *25, 455.*

[38] Brieler, F. J.; Froba, M.; Chen, L.; Klar, P. J.; Heimbrodt, W.; Krug Von Nidda, H. A.; Loidl, A. *Chem. Eur. J.*, **2002**, *8, 185*.

[39] Miffitt, M.; Vali, H.; Eisenberg, A. *Chem. Mater.* **1998**, *10, 1021.*

[40] Tamborra, M. ; Striccoli, M.; Comparelli, R.; Curri, M. L.; Petrella, A.; Agastiano, A. *Nanotechnology* **2004**, *15, S240.*

[40] Bandaranayake,R.J. ; Wen,G.W.; Lin,J.Y.; Jiang,H.X.; Sorensen,C.M. *Appl. Phys. Lett.* **1995**, *67(6), 831.*

[41] Xiao, Q. ; Xiao, C. ; Ouyang, L. *Lumin. J.,* **2008,** *128, 1942***.**

[42] Bargalik – Chory, C.; Remenyi, C.; Dem, C.; Ruster, C.; Hofman, D. M. *J. Phys. Chem.,* **2003**, *1639, 1643.*

[43] Kostic, R.; Romcevic, N.; Comor, M. I.; Romcevic, M.; Grujic –Brojcin, M.; Vodnik, V. V.; Nedeljkovic, J. M. *Mater. Sci Forum,* **2004,** *453, 293.*

.